Concurrent Activation of Kras and Canonical Wnt Signaling Induces Premalignant Lesions That Progress to Extrahepatic Biliary Cancer in Mice

Munemasa Nagao[1], Akihisa Fukuda[1], Mayuki Omatsu[1], Mio Namikawa[1], Makoto Sono[1], Yuichi Fukunaga[1,2], Tomonori Masuda[1], Osamu Araki[1], Takaaki Yoshikawa[1], Satoshi Ogawa[1], Kenji Masuo[1], Norihiro Goto[1], Yukiko Hiramatsu[1], Yu Muta[1], Motoyuki Tsuda[1], Takahisa Maruno[1], Yuki Nakanishi[1], Makoto Mark Taketo[3,4], Jorge Ferrer[5,6,7], Tatsuaki Tsuruyama[2], Yasuni Nakanuma[8], Kojiro Taura[9], Shinji Uemoto[9], and Hiroshi Seno[1]

ABSTRACT

Biliary cancer has long been known to carry a poor prognosis, yet the molecular pathogenesis of carcinoma of the extrahepatic biliary system and its precursor lesions remains elusive. Here we investigated the role of Kras and canonical Wnt pathways in the tumorigenesis of the extrahepatic bile duct (EHBD) and gall bladder (GB). In mice, concurrent activation of Kras and Wnt pathways induced biliary neoplasms that resembled human intracholecystic papillary-tubular neoplasm (ICPN) and biliary intraepithelial neoplasia (BilIN), putative precursors to invasive biliary cancer. At a low frequency, these lesions progressed to adenocarcinoma in a xenograft model, establishing them as precancerous lesions. Global gene expression analysis revealed increased expression of genes associated with c-Myc and TGFβ pathways in mutant biliary spheroids. Silencing or pharmacologic inhibition of c-Myc suppressed proliferation of mutant biliary spheroids, whereas silencing of Smad4/Tgfbr2 or pharmacologic inhibition of TGFβ signaling increased proliferation of mutant biliary spheroids and cancer formation *in vivo*. Human ICPNs displayed activated Kras and Wnt signals and c-Myc and TGFβ pathways. Thus, these data provide direct evidence that concurrent activation of the Kras and canonical Wnt pathways results in formation of ICPN and BilIN, which could develop into biliary cancer.

Significance: This work shows how dysregulation of canonical cell growth pathways drives precursors to biliary cancers and identifies several molecular vulnerabilities as potential therapeutic targets in these precursors to prevent oncogenic progression.

Introduction

Biliary cancer, including cholangiocarcinoma (CCA) and gall bladder carcinoma (GBC), accounts for approximately 3% of all adult malignancies (1). According to their anatomical location, CCAs are classified as either intrahepatic (iCCA), perihilar (pCCA), or distal CCA (dCCA; ref. 2). Recently, the WHO classified iCCA into two subtypes, small duct type and large duct type, based on their different etiologies and clinical behaviors (3). Risk factors for CCA include liver flukes, primary sclerosing cholangitis, hepatolithiasis, choledochal cyst, and viral hepatitis (4). Most biliary cancer is not diagnosed until the late stages, such as the locally advanced or metastatic phases. Most of the currently available chemotherapies for biliary cancer are not sufficiently effective, and the 5-year survival rate of biliary cancer is only 5% to 15% (5, 6). To improve its poor prognosis, the development of novel diagnostic methods and therapeutic strategies is urgently needed. Accordingly, it is important to clarify the molecular mechanism underlying the development of biliary cancer and its precursor lesions.

CCA is considered to develop mainly from two distinct types of precancerous lesions, biliary intraepithelial neoplasm (BilIN) and intraductal papillary neoplasm of the bile duct (IPNB; refs. 7–9). IPNB-like lesions in the gall bladder (GB) are commonly referred to as intracholecystic papillary-tubular neoplasm (ICPN; ref. 10). However, it is not known if these lesions are bona fide precursors of biliary cancer. Furthermore, the molecular pathogenesis of these precursor lesions is still not well understood. This is partly because these precursor lesions have only been recently defined and genetically engineered mouse models (GEM) of these lesions have not yet been well established. GEMs, particularly those that apply the inducible CreER system, are robust tools used in the study of the molecular pathogenesis of human diseases and in the preclinical assessment of novel therapeutic strategies. To date, only a limited number of GEMs for tumors of the extrahepatic biliary system including extrahepatic biliary duct (EHBD) and GB have been

[1]Department of Gastroenterology and Hepatology, Kyoto University Graduate School of Medicine, Sakyo-ku, Kyoto, Japan. [2]Department of Drug Discovery Medicine, Medical Innovation Center, Kyoto University Graduate School of Medicine, Sakyo-ku, Kyoto, Japan. [3]Kitano Hospital, The Tazuke Kofukai Medical Research Institute, Kita-ku, Osaka, Japan. [4]iACT, Kyoto University Hospital, Sakyo-ku, Kyoto, Japan. [5]Centre for Genomic Regulation (CRG), The Barcelona Institute of Science and Technology, Barcelona, Spain. [6]CIBER de Diabetes y Enfermedades Metabólicas Asociadas, Spain. [7]Genetics and Genomics Section, Department of Metabolism, Digestion and Reproduction, National Institute for Health Research (NIHR) Imperial Biomedical Research Centre, Imperial College London, London, United Kingdom. [8]Department of Diagnostic Pathology, Fukui Prefecture Saiseikai Hospital, Fukui, Japan. [9]Division of Hepatobiliary Pancreatic Surgery and Transplantation, Department of Surgery, Kyoto University Graduate School of Medicine, Sakyo-ku, Kyoto, Japan.

Note: Supplementary data for this article are available at Cancer Research Online (http://cancerres.aacrjournals.org/).

Corresponding Author: Akihisa Fukuda, Department of Gastroenterology and Hepatology, Kyoto University, 54 Shogoin-Kawahara-cho, Sakyo-ku, Kyoto 606-8507, Japan. E-mail: fukuda26@kuhp.kyoto-u.ac.jp

Cancer Res 2022;82:1803–17

doi: 10.1158/0008-5472.CAN-21-2176

reported, partly because there is no known tissue-specific driver CreER mouse line for the extrahepatic biliary system.

Although previous whole-genome sequencing (WGS) studies have demonstrated a complex mutational landscape of biliary cancer (11, 12), little is known about the molecular biological significance of each genetic alternation. Several recent studies of murine biliary cancer models have revealed that Pten (13), Smad4/TgfβR2 (14), ErbB-2A (15), Kras, and p53 (16) play prominent roles in biliary tumorigenesis. However, given the heterogenous characteristics of biliary cancer and the variety of mutations, the molecular function of other genes in biliary tumorigenesis has to be taken into consideration. WGS studies have revealed that the incidence of mutations in *Kras* (16.5%) and Wnt-related genes, including *APC* (7.1%), *RNF43* (4.7%), and *CTNNB* (1.3%), are relatively frequent in biliary cancer (17). The incidence of *Kras* mutation is relatively high in both extrahepatic cholangiocarcinoma and intrahepatic cholangiocarcinoma (11). Mutation of *Kras* occurs in 34.2% of BilIN cases (18). According to the International Cancer Genome Consortium, biliary cancer is classified into four subgroups based on mutation status, copy number variants, gene expression, gene methylation, and prognosis. Subtype 2 biliary cancer is reported to have a high gene expression of WNT5B and CTNNB1 (17). In GB cancer, mutation of *CTNNB* is observed in 12% of GBC cases (19). In previous reports, mutations of *CTNNB* were observed in 6 of 11 co-existing BilIN and GB carcinoma cases (20) and in 5 of 26 co-existing IPNB/ITPN and CCA cases (21). However, the role of the Kras and Wnt pathways in biliary tumorigenesis remains elusive.

Therefore, in this study, we aimed to investigate the role of the Kras and canonical Wnt pathways in the tumorigenesis of the extrahepatic biliary system including the EHBD and GB. We found that concurrent activation of the *Kras* and canonical Wnt pathways in adult biliary epithelial cells induced ICPN and BilIN, which could develop into biliary cancer, in mice. This study provides a novel GEM of ICPN and BilIN, establishing them as precursors to biliary cancer. Furthermore, mechanistically, c-Myc contributed to tumorigenesis, whereas the Tgfβ pathway inhibited it.

Materials and Methods

Mice

Experimental animals were generated by crossing *Hnf1b-CreERT2* mice (a gift from Jorge Ferrer, Imperial College; ref. 22), $Kras^{G12D}$ mice (a gift from David Tuveson, Cold Spring Harbor Laboratory, Cold Spring Harbor, NY), $Ctnnb1^{lox(ex3)/+}$ mice (generated as described previously; ref. 23), *Rosa26-LacZ* mice (purchased from The Jackson Laboratory, JAX strain 003309), *Rosa26-tdTomato* mice (purchased from The Jackson Laboratory, JAX strain 007914), $Dclk1^{CreERT2\text{-}IRES\text{-}EGFP}$ mice (24), and *Bmi1-CreERT* (purchased from Jackson Laboratory, JAX strain 010531). Genotyping primers are listed in Supplementary Table S1.

For the induction of Cre-mediated recombination, tamoxifen (Sigma-Aldrich) was administered by oral gavage to Hnf1b-CreERT2 mice at a dose of 400 μg/g body weight per gavage. Time courses are outlined in **Figs. 1B**, **D**, and **2A**. For induction of Cre-mediated recombination, 2 mg of tamoxifen was intraperitoneally injected to *Dclk1CreER*; $Kras^{G12D}$; $Ctnnb1^{lox(ex3)/+}$ and *Bmi1CreER*; $Kras^{G12D}$; $Ctnnb1^{lox(ex3)/+}$ mice once a day over 4 consecutive days. Time courses are outlined in Supplementary Fig. S2A. All experiments involving mice were approved by the animal research committee of Kyoto University.

Histologic analyses and immunostaining

Mouse tissues were performed by perfusion of 4% paraformaldehyde at sacrifice, fixed in 4% paraformaldehyde overnight, dehydrated in 70% ethanol for 2 days, embedded in paraffin, and cut into 5 μmol/L sections. Paraffin-embedded sections were stained with hematoxylin and eosin (H&E). For X-gal staining, isolated bile ducts were incubated for 1 hour in fixative solution (4% formaldehyde, 0.2% glutaraldehyde, 0.02% Nonidet P-40, 5 mmol/L EGTA, 2 mmol/L $MgCl_2$) at 4°C. The tissues were washed twice in PBS and then incubated in a β-galactosidase substrate (5 mmol/L K3[Fe(CN)6], 5 mmol/L K4[Fe(CN)6]×$3H_2O$, 2 mmol/L $MgCl_2$, 0.02% Nonidet P-40, 0.1% Na deoxycholate, and 1 mg/mL X-gal in PBS) in the dark overnight. After fixation, the sections were counterstained with Nuclear Fast Red (Sigma-Aldrich, catalog no. N3020). For IHC, antigen retrieval was performed by boiling the sections in 10 mmol/L citric acid buffer (pH 6.0) or EDTA buffer (pH 8.0) for 15 minutes at 98°C. Blocking was performed by incubating the sections with a blocking solution (Dako, catalog no. X0909). For the primary antibodies, the incubation was performed overnight at 4°C in a humidified chamber. Secondary antibody incubation was conducted for 1 hour at room temperature. Immunoperoxidase labeling was performed using the VECTASTAIN Elite ABC Standard Kit (Vector Laboratories, catalog no. PK-6100). The sections were then colored with diaminobenzidine substrate (Dako, catalog no. K3468) and counterstained with hematoxylin. For immunofluorescence, sections were incubated with a primary antibody overnight at 4°C. The sections were then incubated with a fluorescence-conjugated secondary antibody (Invitrogen) for 1 hour at room temperature. The primary antibodies used in this study are listed in Supplementary Table S2.

Three-dimensional culture

Organoid/spheroid cultures were established from murine EHBD and GB. Mouse EHBD and GB were minced into small pieces and digested with dissociation buffer at 37°C for 15 to 20 minutes. The dissociation buffer consisted of DMEM with 10% FBS, 1 mg/mL collagenase D (Roche Diagnostics Deutschland GmbH), 0.5 mg/mL dispase (Invitrogen), and 40 μg/mL DNase (Roche Diagnostics Deutschland GmbH). The tissue suspension was passed through a 100-μmol/L cell strainer and washed twice by DMEM with 10% FBS. Washed cells were mixed with 15 μL Matrigel per well on a 48-well plate. Passaging was performed at 1:4 to 1:8 split ratios once per week. For passaging, organoids were digested in TrypLE (Invitrogen) for 10 minutes at 37°C. Centrifuged cells were mixed with 15 μL Matrigel per well on a 48-well plate. Expansion Medium (L-WNR Conditioned Medium-based, detailed below) was typically used. Two weeks before the extraction of total RNA or protein, organoids were incubated with Analysis Medium (without FBS, detailed below) and every organoid was passaged at 1.0×10^4 cells/well. 10048-F4 (Selleck Chem, catalog no. S7153) was used as a c-Myc inhibitor in vitro. SB431542 (Tocris Bioscience, catalog no.1614) was used as a Tgfβ inhibitor *in vitro*.

Expansion medium (L-WNR conditioned medium-based)

The Expansion Medium comprised a 50% conditioned medium of L-cell line secreting Wnt3a, R-spondin3, and Noggin (L-WRN CM) supplemented with 10 μmol/L Y-27632 (Tocris Bioscience) and 2 μmol/L SB 431542 (Tocris Bioscience). L-WRN CM was prepared from the L-WRN cell line (ATCC; CRL-3276; ref. 25).

Analysis medium (without FBS)

The Analysis Medium (without FBS) comprised Ad-DMEM/F12 (Invitrogen) supplemented with B27 and N2, 1× Glutamax

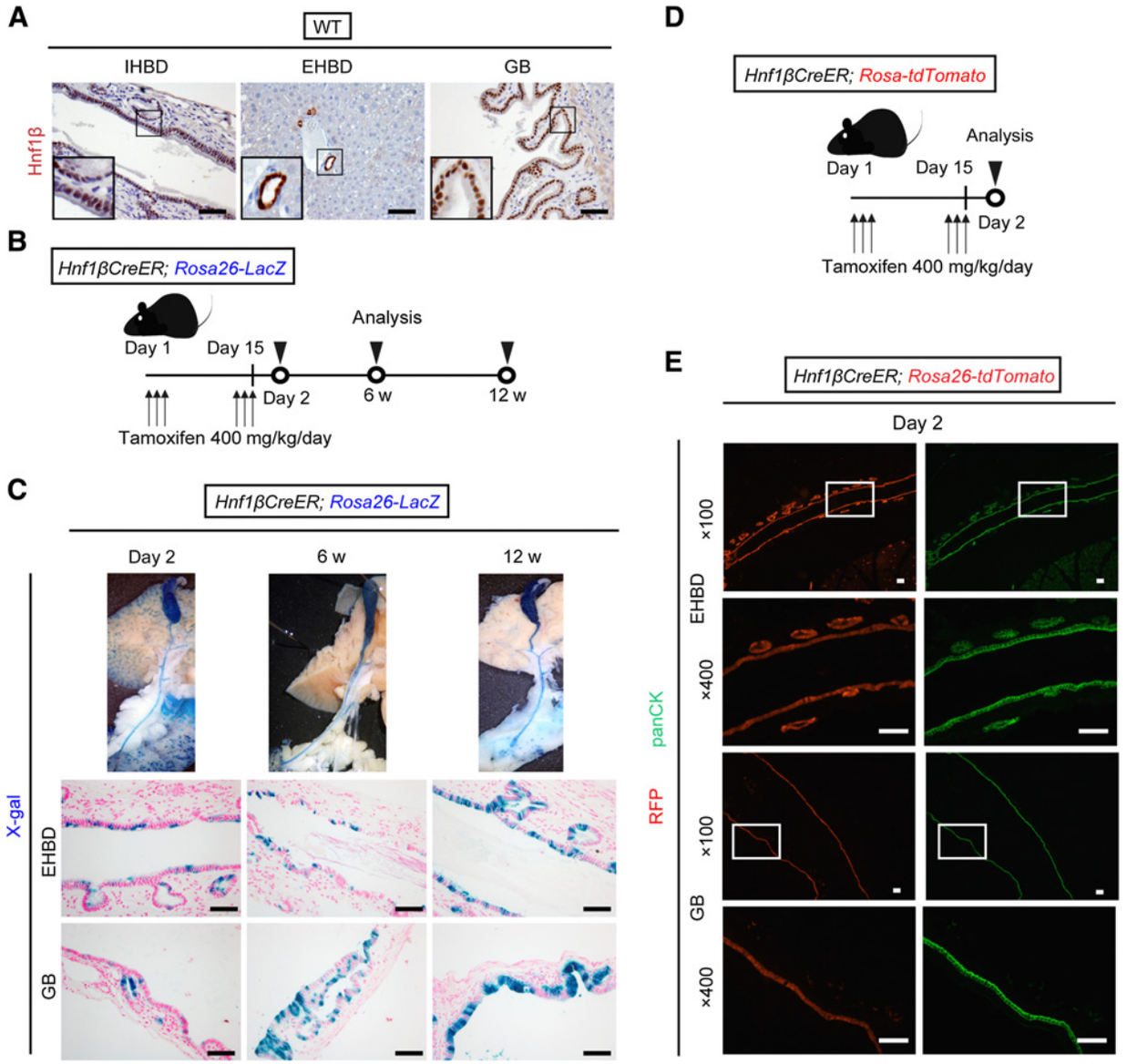

Figure 1.

Hnf1b^{CreER} is a suitable CreER mouse line with high efficiency to perform genetic manipulation in the extrahepatic biliary tract epithelium. **A,** Immunostaining for Hnf1β in the EHBD, IHBD, and GB of wild-type mice ($n = 3$). **B,** Tamoxifen administration schema for lineage tracing experiments using *Hnf1b*^{CreER}*; Rosa26-LacZ* mice. **C,** Macroscopic (top) and microscopic (bottom) images of X-gal staining in *Hnf1b*^{CreER}*; Rosa26-LacZ* mice 2 days ($n = 5$), 6 weeks ($n = 5$), and 12 weeks ($n = 5$) after the last tamoxifen administration. **D,** Tamoxifen administration schema for the experiments using *Hnf1b*^{CreER}*; Rosa26-tdTomato* mice. **E,** Immunostaining for RFP (left) and panCK (right) in *Hnf1b*^{CreER}*; Rosa26-tdTomato* mice at 2 days ($n = 3$) after the last tamoxifen administration. All black or white scale bars, 50 μm.

(Invitrogen), 10 mmol/L HEPES, 1 × penicillin-streptomycin (Invitrogen), 1 mmol/L N-acetylcysteine (Sigma-Aldrich), 10 mmol/L nicotinamide (Sigma-Aldrich), 50 ng/mL EGF (Peprotech), 1 μg/mL Rspondin-1 (Peprotech), 50 ng/mL Wnt3a (Peprotech), 100 ng/mL Noggin (Peprotech), 100 ng/mL FGF10 (Peprotech), and 10 μmol/L Y-27632 (Tocris Bioscience).

Proliferation assay performed by PrestoBlue

For the cell proliferation assay, spheroids (5.0×10^3) were seeded with 10 μL Matrigel per well in 96-well plates. Cell proliferation was evaluated using PrestoBlue Cell Viability Reagent (Invitrogen; catalog no. A13262) following the manufacturer's protocol. On days 1, 3, and 5, the absorbance at 560 and 595 nm was measured using a plate reader.

The values were calculated as suggested by the product protocol: (absorbance at 560 nm spheroid well − absorbance 595 nm spheroid well) − (absorbance 560 nm empty well − absorbance 595 nm empty well)/(absorbance 560 nm spheroid day 1 − absorbance 595 nm spheroid well day 1) − (absorbance 560 nm empty well day 1 − absorbance 595 nm empty well day 1).

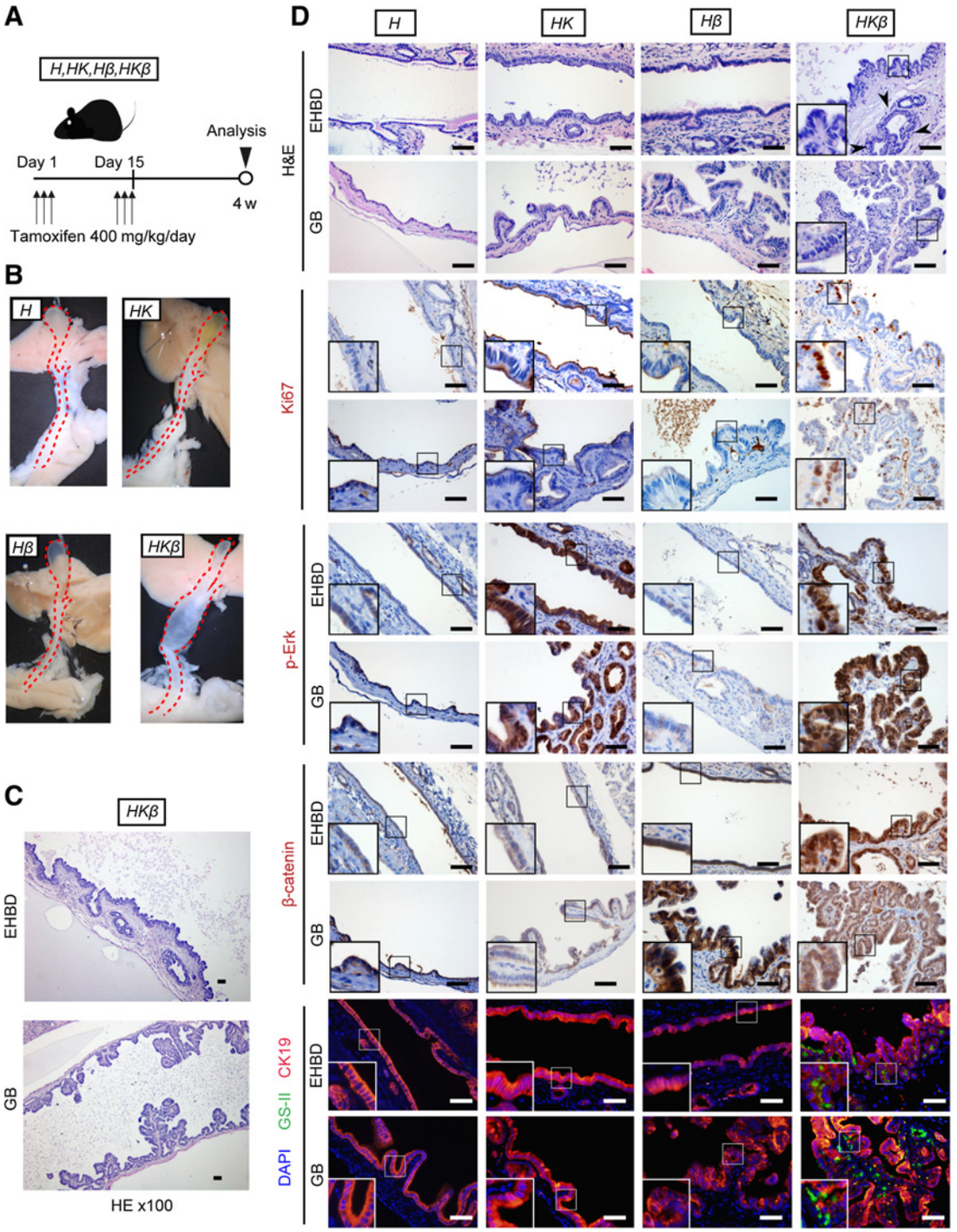

Figure 2.

Concurrent activation of Kras and Wnt pathways induced ICPN and BilIN that resemble human ICPN and BilIN. **A,** Tamoxifen administration schema for the experiments using *Hnf1b*^{CreER}*(H)*, *Hnf1b*^{CreER}; *Kras*^{G12D} *(HK)*, *Hnf1b*^{CreER}; *Ctnnb1*$^{lox(ex3)/+}$ *(Hβ)*, and *Hnf1b*^{CreER}; *Kras*^{G12D}; *Ctnnb1*$^{lox(ex3)/+}$ *(HKβ)* mice (n = 5–7 mice/group). All mice were sacrificed 4 weeks after the last tamoxifen administration. **B,** Macroscopic images of the EHBD in *H*, *HK*, *Hβ*, and *HKβ* mice 4 weeks after the last tamoxifen administration. **C,** H&E staining (low power field) of the EHBD and GB in *HKβ* mice 4 weeks after the last tamoxifen administration. **D,** From the top, H&E staining (high power field), immunostaining for Ki67, p-ERK, β-catenin, and coimmunostaining for DAPI (blue), GS-II (green), and CK19 (red) in the EHBD and GB in *H*, *HK*, *Hβ*, and *HKβ* mice 4 weeks after the last tamoxifen administration. Neoplastic changes were also observed in the peribiliary glands of EHBD in *HKβ* mice (arrowheads). Hyperchromasia, nuclear stratification, and partial loss of nuclear polarity were observed in epithelial cells of BilIN and ICPN lesions in *HKβ* mice (insets). All black or white scale bars, 50 μm.

Proliferation and apoptosis assay by immunostaining

Immunostaining for Ki67 and cleaved Caspase3 was performed in *H*, *HK*, *Hβ*, and *HKβ* spheroids. All cells, Ki67-positive cells, and cleaved Caspase3-positive cells were quantified in a low-power field.

RNA isolation and qRT-PCR

Total RNA was extracted using the RNeasy Micro Kit (Qiagen). Single-strand complementary DNA was synthesized using a ReverTra Ace qPCR RT Kit (TOYOBO). qRT-PCR was performed using SYBR Green Master Mix (Roche Diagnostics Deutschland GmbH) and LightCycler 480 (Roche Diagnostics Deutschland GmbH). The expression levels were standardized by comparing them to the levels of *GAPDH* or *β-actin* (for *c-Myc*). Primer sequences are listed in Supplementary Table S3.

Microarray analysis

The Clariom S Assay (Thermo Fisher Scientific) was used for microarray analysis. Sample preparation, microarray hybridization, and bioinformatics analyses were performed by Macrogen. The quality of RNA extracted from spheroids was examined with an Agilent 2100 bioanalyzer (Agilent Technologies) and a Nanodrop (Thermo Fisher Scientific). The RNA samples were hybridized to the Affymetrix GeneChip Array (Thermo Fisher Scientific). Array data export processing and analysis were performed using Affymetrix GeneChip Command Console Software and Transcriptome Analysis Console (Thermo Fisher Scientific). The raw data were normalized by Affymetrix Power Tools Software (Thermo Fisher Scientific). Unnamed genes were excluded. The gene expression data of the samples were analyzed using gene set enrichment analysis (GSEA) software provided by the Broad Institute of MIT and Harvard University.

Xenograft

For the xenograft model of H, HK, Hβ, and HKβ biliary spheroids, every spheroid was passaged at 5.0×10^4 cells/well. Spheroids were obtained from three wells 3 days after passage. Harvested spheroids were suspended in 50 μL Matrigel + 50 μL Ad-DMEM/F12 and injected subcutaneously into NOD/SCID mice (NOD.CB17-Prkdcscid/J; purchased from The Jackson Laboratory, JAX strain 001303) at one site. After 3 months, tumorigenicity was assessed.

For the xenograft model of shSmad4 and shTgfbr2 *HKβ* biliary spheroids, every spheroid was passaged at 1.0×10^4 cells/well. Spheroids were obtained from the two wells 4 days after passage. Harvested spheroids were suspended in 50 μL Matrigel + 50 μL Ad-DMEM/F12 and injected subcutaneously into NOD/SCID mice at one site. One month later, tumorigenicity was assessed.

DNA extraction

DNA was extracted using the QIAamp DNA Micro Kit (Qiagen) according to the manufacturer's protocol. Sample integrity and yield were assessed by the Nanodrop (Thermo Fisher Scientific) and the Agilent TapeStation. Purified DNA samples were stored at −20°C.

Library preparation and WES

The samples were prepared according to an Agilent SureSelect Target Enrichment Kit preparation guide. The libraries were sequenced with Illumina NovaSeq 6000 sequencer. Whole exome capture was carried out using Agilent's SureSelect Mouse Kit. After DNA quality evaluation, pooled samples were sequenced on Illunima NovaSeq 6000 according to the manufacture's instructions for paired-end 150 bp reads. The average sequencing depth of target region and total mapped reads were summarized in Supplementary Table S4. The Whole exome sequencing was performed by Macrogen.

Exome-sequencing data analysis for SNVs and INDELs calling

Quality check in Raw data (stored as FastQ format) was performed with the FastQC (ver0.11.8). Adapter contamination and low-quality nucleotides are discarded by using Trim Galore (ver0.6.4). Read pairs were mapped to the reference genome GRCm38 using the BWA-MEM (ver0.7.17). Duplicates were trimmed from the reads using the Picard Mark Duplicates (ver2.22.9). Furthermore, we performed base quality score recalibration with Base Recalibrator and ApplyBQSR in GATK (ver4.1.9.0).

After realignment to genome, we identified and filtered variants (SNPs, Indels) using GATK Mutect2 Somatic Mutation Call, GATK Filter Mutect Calls, and GATK Select Variants to guarantee meaningful analysis. Mutations with less than 5% allele frequency, low (<5) number of read, and low (<2) number of read with mutation in xenografted tumor were excluded from analysis. More than 10bp Indel, Known SNPs and Indels registered in Mouse Genomes Project, and silent mutations were excluded from analysis. The filtered mutations were annotated with VEP (ver96). Finally, the mutation spectrum of the final variant set was analyzed with the R package maftools (ver2.6.0). The WES data analysis was performed by cBioinformatics.

Lentivirus transduction and infection

The silencing of c-Myc was achieved using pLKO-shMyc (MISSION shRNA NM_010849 TRCN0000042517, purchased from Sigma-Aldrich), the silencing of Smad4 was attained using pLKO-shSmad4 (MISSION shRNA NM_008540 TRCN0000025881, purchased from Sigma-Aldrich), and the silencing of Tgfbr2 was attained using pLKO-shTgfbr2 (MISSION shRNA NM_009371 TRCN0000294600, purchased from Sigma-Aldrich). To produce lentiviruses, HEK293T cells were transfected with the targeting plasmid, pCAG-HIVgp, and pCMV-VSV-G-RSV-Rev (donated by Dr. Hiroyuki Miyoshi, RIKEN BioResource Center) plasmids. The culture supernatants were collected 48 hours after transfection, filtered, concentrated by PEG-it (System Biosciences, catalog no. LV810A-1), and resuspended in Hanks' balanced salt solution. Infection was performed in the presence of polybrene (8 μg/mL) for 6 hours, followed by selection with puromycin 1 μg/mL. For the proliferation analysis of the spheroids that silenced c-Myc, Smad4, and Tgfbr2, the spheroid was passaged at 2.0×10^3 cells/well after selection by puromycin.

The Cancer Genome Atlas database

The data and analysis results can be explored through The Cancer Genome Atlas (TCGA) Data Portal from the cBioPortal on the Cancer Genomics website (https://www.cbioportal.org/).

Statistical analysis

Data are presented as mean ± SEM. When $n = 3$ per each group, dot plots are also represented. The two-tailed Student *t* test was performed to analyze the statistical difference between two groups. To determine statistically significant associations between treatment groups versus a control group or between the other groups versus a control group, the data were statistically analyzed with ANOVA followed by the Dunnett test. *P* value of less than 0.05 was considered statistically significant. All statistical analyses were performed with either JMP 15 (SAS Institute Inc.) or GraphPad Prism, version 6.0 (GraphPad).

Study approval

All mouse experiments were approved by the animal research committee of Kyoto University (180260) and performed in accordance with Japanese government regulations. We used 12 surgically resected ICPN tissues that were obtained from patients admitted to Kyoto University Hospital and that were stored in the hospital. The patient samples were only used for immunohistochemistry and the Ethics Committee of Kyoto University approved the use of patient samples for this experiment without requiring written informed consent. Informed consent was obtained in the form of opt-out on the website. This research conformed to the provisions of the Declaration of Helsinki. The study protocol (G1200–1 and R2904) was approved by the Ethics Committee of Kyoto University.

Data availability

All original microarray data were deposited in the Gene Expression Omnibus at National Center for Biotechnology Information (GSE191072). The whole exome sequence data were deposited in the DDBJ Sequence Read Archive (DRA) database (DRA013309). The data that support the findings of this study are included in this article and its Supplementary Table or available from the corresponding author upon reasonable request.

Results

Hnf1β was expressed in the extrahepatic biliary system including the EHBD and GB

To perform genetic manipulation in the extrahepatic biliary tract epithelium including the EHBD and GB, we first sought to determine a suitable CreER mouse line. Given that HNF1β expression has been reported to be restricted to biliary duct epithelial cells in the normal murine liver (26), we performed immunostaining (IHC) for Hnf1β to determine the expression pattern of Hnf1β in the extrahepatic biliary tract epithelium including the EHBD and GB in adult mice. Hnf1β was robustly expressed in the EHBD, IHBD and GB epithelial cells in adult wild type mice (**Fig. 1A**).

To assess the efficiency of Cre expression in Hnf1β positive EHBD cells in *Hnf1b*^{CreER} mice, we generated *Hnf1b*^{CreER}*; Rosa26 LacZ* mice and performed lineage-tracing experiments by the administration of tamoxifen (**Fig. 1B**). Macroscopically and histologically, the EHBD and GB epithelial cells were *Hnf1b*-lineage labeled in *Hnf1b*^{CreER}*; Rosa26 LacZ* mice at 2 days, 6 weeks, and 12 weeks after the last administration of tamoxifen (**Fig. 1C**). We also generated *Hnf1b*^{CreER}*; Rosa26 tdTomato* mice and assessed *Hnf1b*-lineage labeled efficiency (**Fig. 1D**). Almost all EHBD and GB epithelial cells, which were positive for cytokeratin (CK), were *Hnf1b*-lineage labeled on day 2 after the last tamoxifen administration (**Fig. 1E**). These results indicate that the *Hnf1b*^{CreER} mouse is a suitable CreER mouse line with high efficiency for genetic manipulation in the extrahepatic biliary tract epithelium including the EHBD and GB.

Concurrent activation of the Kras and canonical Wnt pathways induced ICPN and BilIN in mice

We next investigated the functional role of Kras and canonical Wnt signal activation and the effect of concurrent activation of both pathways on tumorigenesis of the extrahepatic biliary system using *Hnf1b*^{CreER} mice. In a previous report, conditional knockout of *exon3 of Ctnnb* induced the stabilization of β-catenin or constitutive activation of the Wnt/β-catenin signaling pathway in a mouse model (23). We crossed *Kras*^{G12D} mice and/or *Ctnnb1*$^{lox(ex3)/+}$ mice with *Hnf1b*^{CreER} mice to generate *Hnf1b*^{CreER}*(H)*, *Hnf1b*^{CreER}; *Kras*^{G12D} *(HK)*, *Hnf1b*^{CreER}; *Ctnnb1*$^{lox(ex3)/+}$ *(Hβ)*, and *Hnf1b*^{CreER}; *Kras*^{G12D}; *Ctnnb1*$^{lox(ex3)/+}$ *(HKβ)* mice. Four weeks after the last tamoxifen administration, the biliary tract was analyzed (**Fig. 2A**). Macroscopically, the EHBD of *HKβ* mice was dilated, whereas that of *H*, *HK*, and *Hβ* mice appeared normal (**Fig. 2B**). H&E staining demonstrated an almost normal appearance of the GB and EHBD epithelial cells in *H* mice and a minimal neoplastic change in *Hβ* and *HK* mice. In contrast, *HKβ* mice (6/6 mice) displayed microscopic papillary neoplasms, which resembled human BilIN in the EHBD, and papillary neoplasm, which resembled human ICPN in the GB (**Fig. 2C** and **D**). Neoplastic changes were also observed in the peribiliary glands of the EHBD in *HKβ* mice. Hyperchromasia, nuclear stratification, and partial loss of nuclear polarity were observed in the epithelial cells of the BilIN and ICPN lesions in *HKβ* mice. Ki67 staining revealed proliferative cells in these lesions in *HKβ* mouse (**Fig. 2D**). EHBD and GB epithelial cells demonstrated increased expression of pErk in both *HK* and *HKβ* mice (**Fig. 2D**). Nuclear accumulation or cytoplasmic staining of β-catenin was observed in the EHBD and GB epithelial cells in both *Hβ* and *HKβ* mice (**Fig. 2D**). These data indicated increased activation of the Kras and Wnt signaling pathways in EHBD and GB epithelial cells in *HKβ* mice.

To better characterize BilIN and ICPN in *HKβ* mice, mucin IHC was performed. Muc1 was positive in biliary epithelial cells in *H*, *Hβ*, *HK*, and *HKβ* mice, whereas muc2 and muc5AC were negative (Supplementary Fig. S1A). Staining for Griffonia simplicifolia lectin II (GSII lectin), which is an alternate marker for muc6 in mice and is indicative of the pyloric gland type (27), revealed that GSII was partially expressed in BilIN and ICPN in *HKβ* mice (**Fig. 2D**). Staining for Ulex europaeus agglutinin I (UEA-1), an indicative marker for the gastric foveolar type in mice (28), revealed that UEA-1 was partially expressed in BilIN and ICPN in *HKβ* mice (Supplementary Fig. S1B). Given that both GSII and UEA-1 were positive in *HKβ* mice, these ICPN lesions resembled human gastric type ICPN.

To compare with other Cre mouse strains, we used *Dclk1CreER* and *Bmi1-CreER* mouse lines and generated *Dclk1CreER*; *Kras*^{G12D}; *Ctnnb1*$^{lox(ex3)/+}$ *(DKβ)* and *Bmi1CreER*; *Kras*^{G12D}; *Ctnnb1*$^{lox(ex3)/+}$ *(BKβ)* mice, respectively. In both *DKβ and BKβ* mice, BilIN-like lesions and ICPN-like lesions were formed in the EHBD and GB, respectively, 4 weeks after tamoxifen administration (Supplementary Figs. S2A–S2C).

Therefore, these data indicate that concurrent activation of the Kras and canonical Wnt pathways results in the development of gastric type ICPN and BilIN of EHBD in mice.

Establishment of spheroids derived from murine mutant GB and EHBD and characterization of their gene expression profiles

To provide insights into the underlying molecular mechanism whereby activation of the Kras and Wnt pathways cooperatively induce ICPN and BilIN in the EHBD of *HKβ* mice, we sought to perform global gene expression analysis of mutant biliary epithelium. However, it was difficult to isolate the extrahepatic biliary epithelium from mouse tissue. Therefore, we applied a 3D culture system of biliary spheroids *in vitro*. We established biliary spheroids derived from the EHBD and GB of *H*, *HK*, *Hβ*, and *HKβ* mice 4 weeks after the last tamoxifen administration (**Fig. 3A**). We confirmed the recombination of *Kras*^{G12D} allele and *Ctnnb1*$^{lox(ex3)/+}$ allele in *H*, *HK*, *Hβ*, and *HKβ* biliary spheroids by genotyping with PCR (Supplementary Figs. S3A–S3C). These spheroids were roundish and did not show any apparent morphologic differences between genotypes (**Fig. 3B**). Proliferation analysis revealed that *HKβ* biliary spheroids grew significantly faster than *H*, *HK*, and *Hβ* biliary spheroids (**Fig. 3C**). Moreover, we

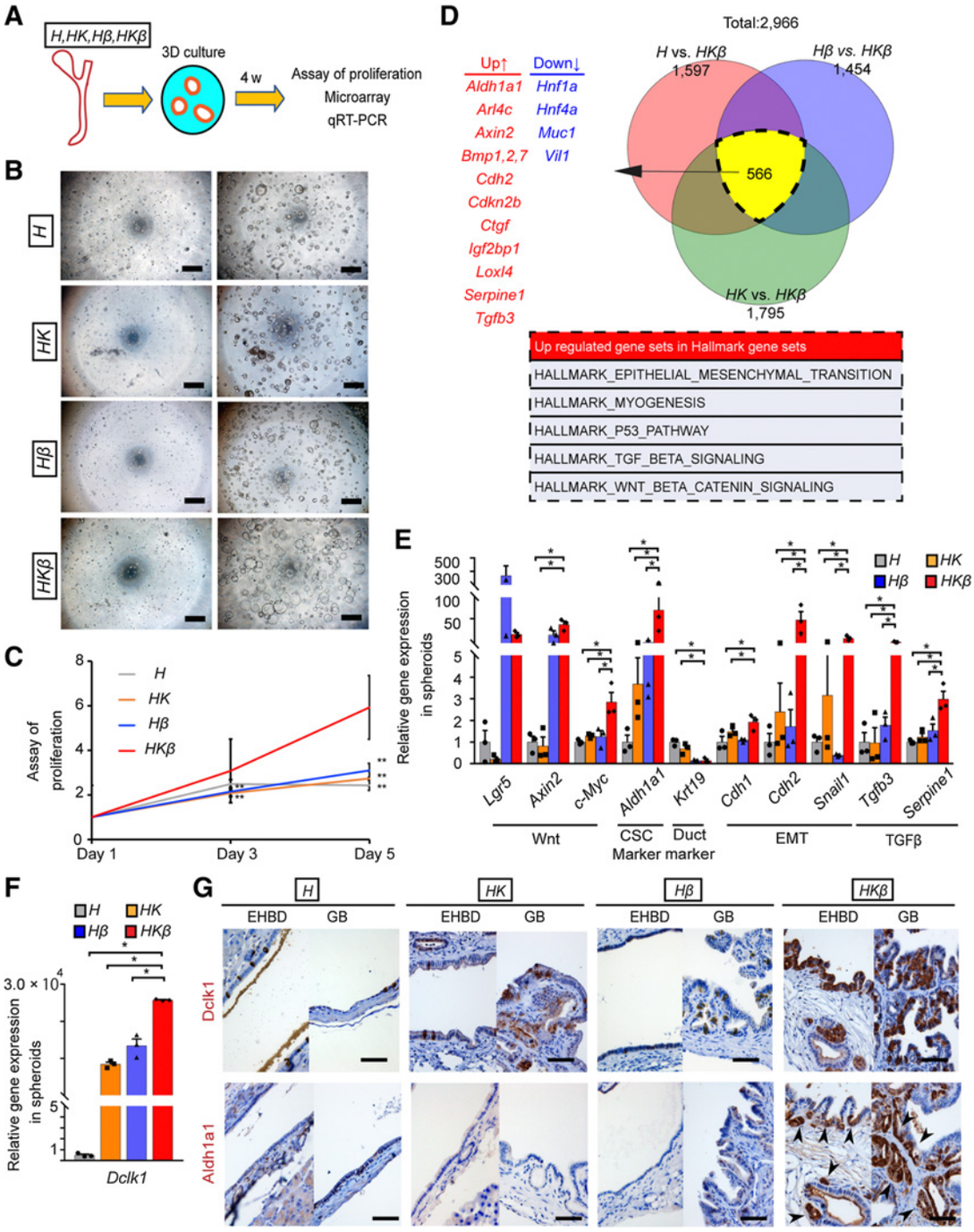

Figure 3.

Expression of Wnt signaling pathway, c-Myc, CSC markers, and Tgfβ pathway was increased in *HKβ* biliary spheroids. **A,** Schema of biliary spheroids established from EHBD and GB in *H*, *HK*, *Hβ*, and *HKβ* mice 4 weeks after the last tamoxifen administration ($n = 3$ mice/group). **B,** Microscopic images of *H*, *HK*, *Hβ*, and *HKβ* biliary spheroids on day 1 and day 5 after passage. Scale bars, 500 μm. **C,** Assay of the proliferation of *H*, *HK*, *Hβ*, and *HKβ* biliary spheroids on day 1, day 3, and day 5 after passage ($n = 3$/group). The assay of proliferation was performed using PrestoBlue. The values were calculated as described in Materials and Methods. Data are mean ± SEM. Analyzed by one-way ANOVA with Dunnett test (vs. *HKβ* spheroids; *, $P < 0.05$; **, $P < 0.01$). **D,** Top, commonly high fold change (>2 log, <−2 log) expression genes on microarray analysis in *HKβ* biliary spheroids. Bottom, upregulated gene sets on Hallmark gene set of GSEA in *HKβ* spheroids. FDR, $q < 0.25$ (vs. *HKβ* spheroids). **E** and **F,** qRT-PCR analysis of *H*, *HK*, *Hβ*, and *HKβ* biliary spheroids ($n = 3$/group). Data are shown as individual data points and the mean ± SEM for each experimental group. Analyzed by one-way ANOVA with Dunnett test (vs. *HKβ* spheroids; *, $P < 0.05$). **G,** Immunostaining for Dclk1 (top) and Aldh1a1 (bottom) in the EHBD and GB in *H*, *HK*, *Hβ*, and *HKβ* mice 4 weeks after the last tamoxifen administration. Aldh1a1 was expressed at a crypt-like location between BilIN in EHBD and the inner epithelial cells of ICPN in *HKβ mice* (arrowheads). Scale bars, 50 μm.

performed immunostaining for Ki67 and cleaved caspase3. The ratio of Ki67 positive proliferative cells was significantly higher in *HKβ* biliary spheroids than *H*, *HK*, and *Hβ* spheroids. On the other hand, the ratio of cleaved caspase 3 positive apoptotic cells in *HKβ* biliary spheroids was lower than *H*, *HK*, and *Hβ* biliary spheroids, although it did not reach statistical significance (Supplementary Figs. S4A–S4C). Therefore, we concluded that the high proliferation contributes to the increased growth of *HKβ* biliary spheroids.

Next, we determined the gene expression profile of *H*, *HK*, *Hβ*, and *HKβ* biliary spheroids by genome-wide microarray analysis. Microarray analysis revealed the molecules with high fold change (>2 log or <−2 log), which included 1,597 genes in *HKβ* spheroids vs. *H* spheroids, 1,795 genes in *HKβ* spheroids versus *HK* spheroids, and 1,454 genes in *HKβ* spheroids versus *Hβ* spheroids. Commonly high fold change (>2 log or <−2 log) expression in *HKβ* spheroids compared to *H*, *HK*, and *Hβ* spheroids included 566 genes (**Fig. 3D**). Upregulated genes in *HKβ* spheroids included *Aldh1a1*, *Arl4c*, *Axin2*, *Bmp1*, *Bmp2*, *Bmp7*, *Cdh2*, *Cdkn2b*, *Ctgf*, *Igf2bp1*, *Loxl4*, *Serpine1*, and *Tgfβ3*. Downregulated genes in *HKβ* spheroids included *Hnf1α*, *Hnf4a*, and *Muc1*. Other genes are listed in Supplementary Data S1. GSEA revealed gene sets corresponding to epithelial–mesenchymal transition (EMT), myogenesis, and TGFβ, p53, and Wnt signaling as commonly enriched signatures in *HKβ* spheroids compared with other genotypes in a "Hallmarks" compilation (**Fig. 3D**). qRT-PCR analysis revealed that the expression of *c-Myc*, *Aldh1a1*, *Cdh2*, *Snail1*, *Tgfb3*, *Serpine1*, and *Dclk1* was significantly ($P < 0.05$) upregulated in *HKβ* spheroids compared to *H*, *HK*, and *Hβ* spheroids (**Fig. 3E** and **F**).

The expression of *Axin2* reflects Wnt/β-catenin activity (29). High expression of *Cdh2* and *Snail1* indicates the tendency of EMT. *Aldh1a1* and *Dclk1* are known cancer stem cell (CSC) markers (24, 30). *Serpine1* is known a target gene of the Tgfβ signaling pathway and encodes plasminogen activator inhibitor-1 (PAI-1; ref. 31). These results indicated that *HKβ* biliary spheroids harbor enhanced features of the Wnt/β-catenin signaling pathway, c-Myc, CSC, EMT, and the Tgfβ signaling pathway compared with *H*, *HK*, and *Hβ* biliary spheroids.

We then performed IHC analysis in murine the EHBD and GB tissue for CSC markers, including Dclk1 and Aldh1a1. Dclk1 was expressed in a small subset of epithelial cells of the EHBD and GB in *H*, *HK* and *Hβ* mice, whereas Dclk1 was strongly expressed in most BilIN and ICPN in *HKβ* mice. Aldh1a1 was not expressed in EHBD and GB in *H*, *HK*, and *Hβ* mice, whereas Aldh1a1 was expressed at a crypt-like location between BilIN in EHBD and in the inner epithelial cells of ICPN in *HKβ* mice (**Fig. 3G**). These results, together with the microarray data above, indicated that coactivation of Kras and canonical Wnt leads to higher tumorigenic potential in mouse biliary tracts.

ICPN and BilIN have a malignant potential to progress to biliary cancer

We next investigated whether BilIN and ICPN in *HKβ* mice were precancerous lesions. Longer-term analysis of *HKβ* mice was impossible, because *HKβ* mice died at 6 to 8 weeks of age after tamoxifen treatment. Given that Hnf1*β* is also expressed in the lung, pancreatic duct, intrahepatic bile duct, and intestinal epithelium (32), we histologically analyzed the intestine, pancreas, liver, and lung in *HKβ* mice 4 and 6 weeks after administration of tamoxifen. We observed massive adenomas in the intestine and focal nodular adenocarcinoma in the lung, whereas pancreas and liver were almost normal in *HKβ* mice 4 and 6 weeks after administration of tamoxifen (Supplementary Fig. S5). *HKβ* mice died due to massive intestinal adenomas. Therefore, we performed xenograft experiments using biliary spheroids developed from the EHBD and GB of *H*, *HK*, *Hβ*, and *HKβ* mice (**Fig. 4A**). Notably, xenograft tumors developed in two out of 24 cases of *HKβ* biliary spheroids approximately 3 months after the injection of spheroids, whereas no xenograft tumors developed from *H*, *HK*, and *Hβ* biliary spheroids (**Fig. 4B** and **C**). Histologically, these xenograft tumors were well-differentiated adenocarcinoma expressing CK19 (**Fig. 4D**). Ki67 staining revealed a high proliferation of xenograft tumors in the cancer cells developed from *HKβ* biliary spheroids.

To investigate the mutational profiles of the xenograft tumors developed from mutant biliary spheroids, we performed WES analysis using two sets of biliary spheroids; two original mutant biliary spheroids and corresponding xenograft biliary cancer spheroids. The WES analysis revealed 10 common additional gene mutations that were observed in the xenograft biliary cancer spheroids but not in the original biliary mutant spheroids in both sets (Supplementary Figs. S6A–S6D).

These results indicated that BilIN in the EHBD and ICPN in *HKβ* mice are bona fide precancerous lesions with a malignant potential to become an adenocarcinoma although at a low frequency *in vivo*.

C-myc is a critical mediator for *HKβ* biliary spheroid growth

Given that c-Myc expression was significantly increased in *HKβ* biliary spheroids compared to *H*, *HK* and *Hβ* biliary spheroids, we subsequently focused on c-Myc (**Fig. 3E**). IHC analysis revealed that c-Myc was expressed in BilIN of the EHBD and ICPN in *HKβ* mice (**Fig. 5A**). Given that c-Myc is known to be located downstream of both Kras and Wnt signaling pathways, and is important for tumor growth (33), we hypothesized that c-Myc plays a critical role in the growth of *HKβ* biliary spheroids. To investigate the functional role of c-Myc in *HKβ* tumorigenesis, we silenced c-Myc in *HKβ* biliary spheroids. The silencing of c-Myc markedly suppressed the growth of *HKβ* biliary spheroids compared to the controls (**Fig. 5B** and **C**). Expression of *Axin2*, *c-Myc*, and *Aldh1a1* was significantly decreased by the silencing of c-Myc in *HKβ* biliary spheroids (**Fig. 5D**).

To further validate the effect of c-Myc inhibition on the growth of *HKβ* biliary spheroids, we performed pharmacologic inhibition of c-Myc in *HKβ* biliary spheroids using 10058-F4, an inhibitor of c-Myc-Max dimerization (34). Administration of c-Myc inhibitor markedly suppressed the growth of *HKβ* biliary spheroids compared with the nontreated controls (**Fig. 5E** and **F**). We performed Myc inhibitor experiments using normal biliary spheroids (*H*) as a negative control. We found that administration of 100 μmol/L 10058-F4 suppressed more effectively the growth of *HKβ* biliary spheroids than that of *H* spheroids. On the other hand, the range of suppression by administration of 50 or 150 μmol/L 10058-F4 was not different between *H* and *HKβ* spheroids (Supplementary Figs. S7A–S7C). Thus, we concluded that Myc inhibitor suppressed more effectively the growth of *HKβ* spheroids than *H* spheroids. These results defined c-Myc as a critical mediator for the growth of *HKβ* biliary spheroids.

Tgfβ signaling pathway suppresses the growth of *HKβ* biliary spheroids

Given that the Tgfβ signaling pathway was also upregulated in *HKβ* biliary spheroids compared with *H*, *HK*, and *Hβ* biliary spheroids by GSEA analysis, we next focused on Tgfβ signaling (**Fig. 3D**). IHC analysis revealed that p-Smad3, located downstream of the canonical Tgfβ pathway, was expressed in the nucleus of BilIN in the EHBD and ICPN in *HKβ* mice (**Fig. 6A**). The Tgfβ signaling pathway is generally known to play an important role as a tumor suppressor at an early stage of tumorigenesis, whereas it functions as a tumor promoter at an advanced stage of tumorigenesis. We hypothesized that the Tgfβ

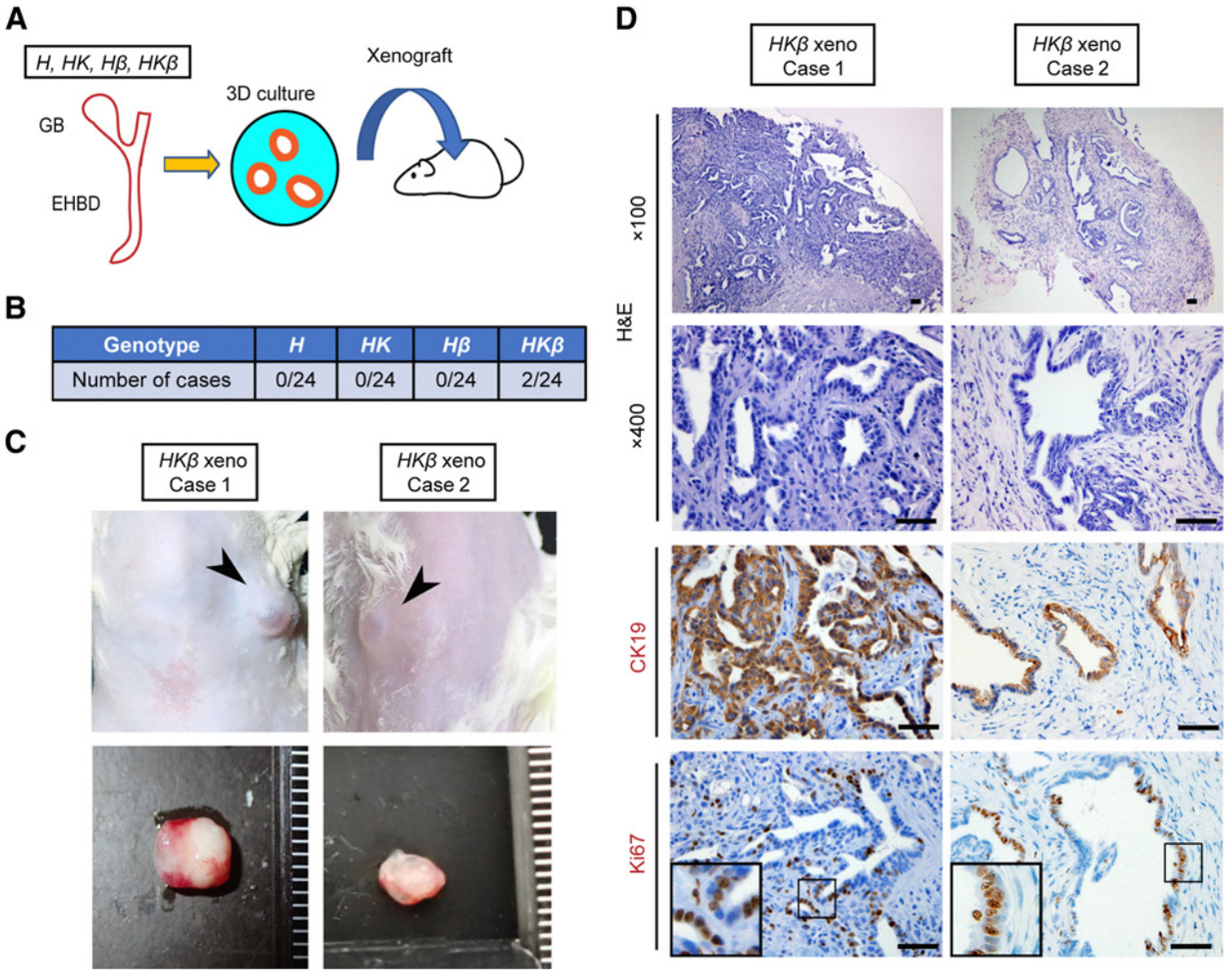

Genotype	*H*	*HK*	*Hβ*	*HKβ*
Number of cases	0/24	0/24	0/24	2/24

Figure 4.

ICPN and BilIN have a malignant potential to progress to biliary cancer. **A,** Schema of the xenograft experiments of *H*, *HK*, *Hβ*, and *HKβ* biliary spheroids ($n = 24$/group). **B,** Xenograft tumors develop in two out of 24 cases of *HKβ* biliary spheroids 3 months after injection of the spheroids. **C,** Macroscopic images of the xenograft tumors. The xenograft tumors are indicated by arrowheads (top). One scale, 1 mm (bottom). **D,** From the top, H&E staining (top, low power field; bottom, high power field) and immunostaining for CK19 and Ki67 in the xenograft tumors. Scale bars, 50 μm.

signaling pathway plays a role in the growth of *HKβ* biliary spheroids. To investigate the functional role of the Tgfβ signaling pathway in the growth of *HKβ* biliary spheroids, we silenced *Smad4* in *HKβ* biliary spheroids. qRT-PCR confirmed that expression of *Smad4* was 79% downregulated in *Smad4* silenced *HKβ* biliary spheroids (Supplementary Fig. S8A). Expression of *Serpine1*: target gene of the Tgfβ signaling pathway was also downregulated in *Smad4* silenced *HKβ* biliary spheroids. Silencing of *Smad4* markedly increased the growth of *HKβ* biliary spheroids compared with the controls (**Fig. 6B** and **C**). To further investigate the functional role of Tgfβ signaling pathway in the growth of *HKβ* biliary spheroids, we silenced *Tgfbr2* in *HKβ* biliary spheroids. qRT-PCR analysis confirmed that the expression of *Tgfbr2* was 79% downregulated in *Tgfbr2*-silenced *HKβ* biliary spheroids. Silencing of *Tgfbr2* markedly increased the growth of *HKβ* biliary spheroids compared with controls (Supplementary Figs. S8B–S8D).

We also performed chemical inhibition of the Tgfβ signaling pathway by administering an inhibitor of the Tgfβ signaling pathway, SB431542 (35), in *HKβ* biliary spheroids. We treated *HKβ* biliary spheroids with SB431542 and analysis of proliferation and qRT-PCR was performed. Growth of *HKβ* biliary spheroids was markedly increased when treated with 1 or 10 μmol/L SB431542 compared with the controls (**Fig. 6D** and **E**). qRT-PCR confirmed that expression of *Dclk1*, *TgfbR1*, *Serpine1*, and *Cdh2* was significantly downregulated in *HKβ* biliary spheroids treated with SB431542 (**Fig. 6F**). We performed chemical inhibition experiments using normal biliary spheroids (*H*) as a negative control. We found that administration of 1 or 10 μmol/L SB431524 increased more effectively the growth of *HKβ* spheroids than that of *H* spheroids. Therefore, we concluded that TGFβ inhibitor increased more effectively the growth of *HKβ* spheroids than *H* spheroids (Supplementary Figs. S7D–S7G). These results further demonstrated that the Tgfβ signaling pathway functions as a suppressive mediator for the growth of *HKβ* biliary spheroids.

Tgfβ signaling pathway suppressed the progression of BilIN and ICPN into biliary cancer

We hypothesized that the Tgfβ pathway also inhibits the progression of BilIN and ICPN into biliary cancer. Accordingly, we performed xenograft experiments using *Smad4*-silenced *HKβ* biliary spheroids

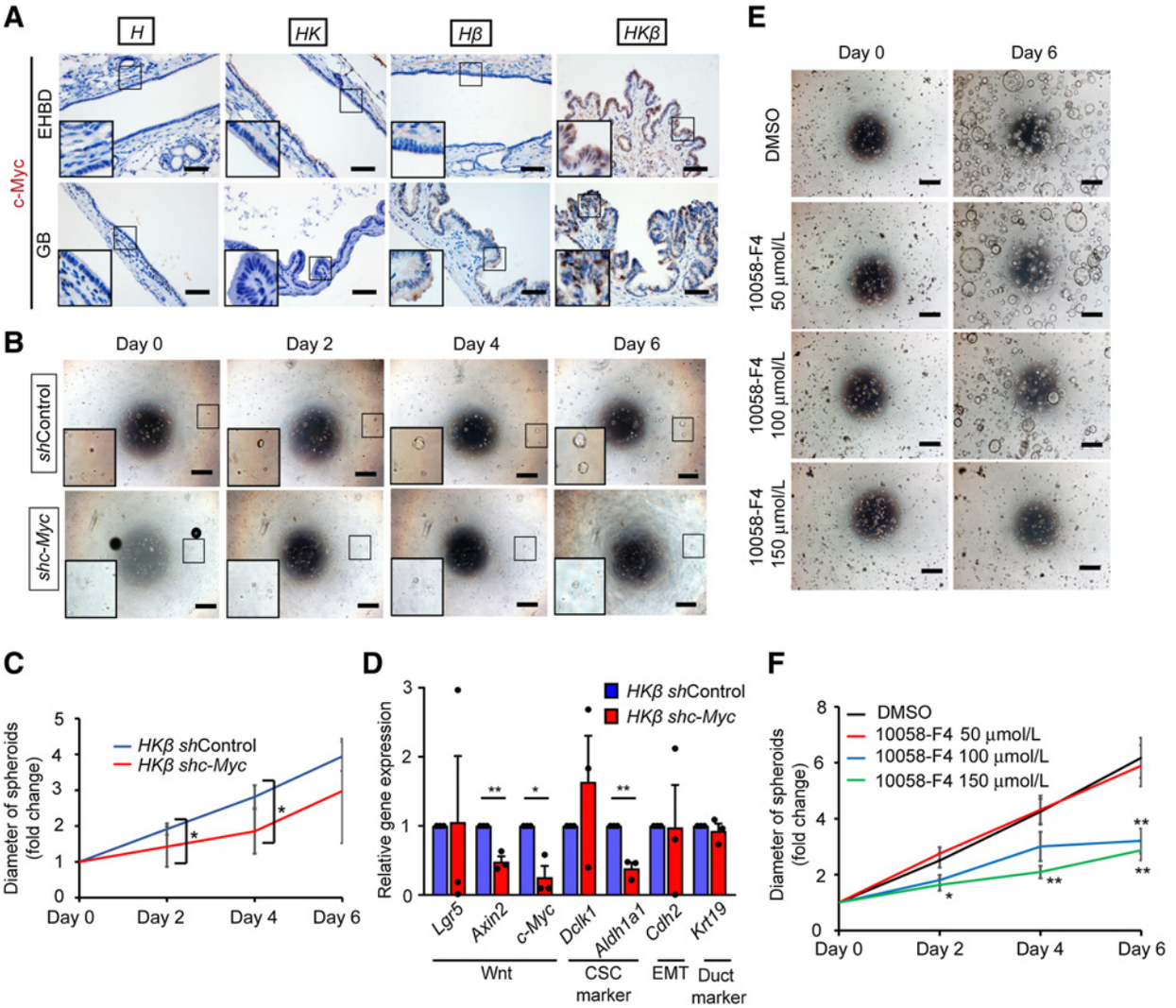

Figure 5.

c-Myc is a critical mediator for the growth of *HKβ* biliary spheroids. **A,** Immunostaining for c-Myc in the EHBD and GB in *H*, *HK*, *Hβ*, and *HKβ* mice 4 weeks after the last tamoxifen administration. Scale bars, 50 μm. **B,** Microscopic images of control and *c-Myc* silenced *HKβ* biliary spheroids on day 0, day 2, day 4, and day 6 after passage. Scale bars, 500 μm. **C,** Diameter (fold change) of control ($n = 3$) and *c-Myc*–silenced ($n = 3$) *HKβ* biliary spheroids on day 0, day 2, day 4, and day 6 after passage. Data are mean ± SEM. Analyzed by Student *t* test. *, $P < 0.05$. **D,** Relative gene expression of *c-Myc* silenced *HKβ* biliary spheroids ($n = 3$) compared with the control spheroids ($n = 3$) on day 6. Data are shown as individual data points and the mean ± SEM for each experimental group. Analyzed by Student *t* test. *, $P < 0.05$; **, $P < 0.01$. **E,** Microscopic images of DMSO, 50, 100, and 150 μmol/L c-Myc inhibitor-treated *HKβ* biliary spheroids on day 0 and day 6 after treatment. Scale bars, 500 μm. **F,** Diameter (fold change) of DMSO, 50, 100, and 150 μmol/L c-Myc inhibitor-treated *HKβ* spheroids on day 0, day 2, day 4, and day 6 after treatment ($n = 3$/group). Data are mean ± SEM. Analyzed by one-way ANOVA with Dunnett test (vs. DMSO). *, $P < 0.05$; **, $P < 0.01$.

(**Fig. 6G**). Notably, xenograft tumors developed in five out of nine cases of *Smad4*-silenced *HKβ* biliary spheroids 1 month after the injection of *Smad4*-silenced the *HKβ* biliary spheroids, whereas no xenograft tumors developed from the control *HKβ* biliary spheroids (**Fig. 6H**). Histologically, xenograft tumors comprised tubular adenocarcinomas expressing CK19 and Ki67 (**Fig. 6H**). The xenograft tumors did not express Smad4 and were negative upon periodic acid-Schiff staining. To further investigate whether Tgfβ pathway inhibits the progression of BilIN and ICPN into biliary cancer, we performed xenograft experiments using *Tgfbr2*-silenced *HKβ* biliary spheroids. We found that xenograft tumors developed in 6 of 18 mice injected with *Tgfbr2*-silenced *HKβ* biliary spheroids 1 month after the injection, whereas no xenograft tumors developed in 18 control mice injected with *HKβ* biliary spheroids (Supplementary Figs. S8E and S8F). These data indicate that the Tgfβ pathway suppresses the progression of BilIN and ICPN into biliary cancer.

Gene expression of human gastric type ICPN and biliary cancer

To investigate whether murine ICPN in *HKβ* mice resembled human ICPNs, we performed IHC analysis using resected human gastric type ICPN samples. Both p-ERK and nuclear β-catenin were expressed in serial sections in 7 of 12 human gastric ICPN cases (**Fig. 7A**). These results suggested that the KRAS and WNT signaling pathways were activated in human ICPNs. Human ICPNs also

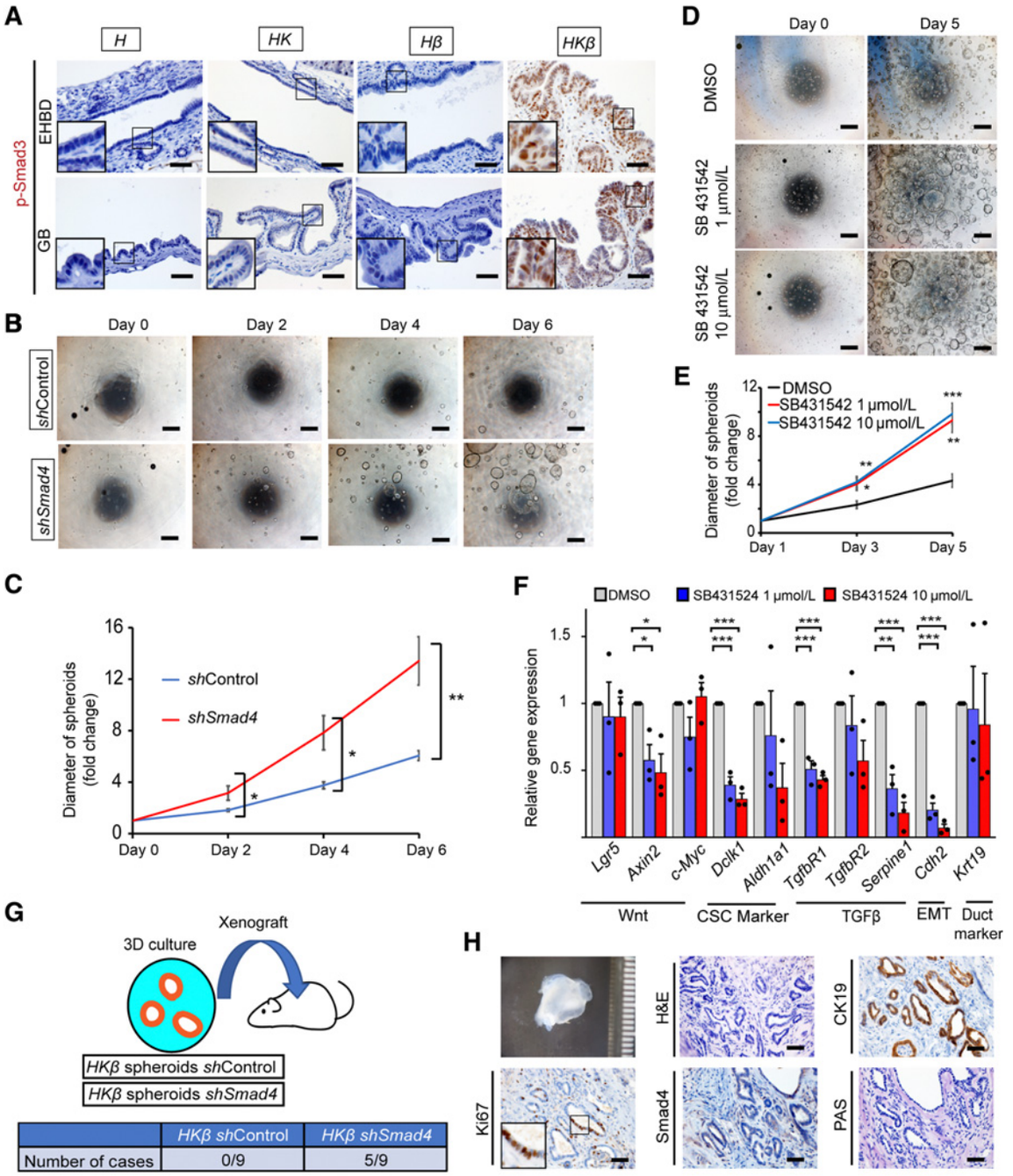

	HKβ shControl	HKβ shSmad4
Number of cases	0/9	5/9

Figure 6.

Tgfβ signaling pathway suppresses the growth of *HKβ* biliary spheroids and the progression of BilIN and ICPN into biliary cancer. **A,** Immunostaining for p-Smad3 in the EHBD and GB in *H*, *HK*, *Hβ*, and *HKβ* mice 4 weeks after the last tamoxifen administration. **B,** Microscopic images of the control and the *Smad4* silenced *HKβ* biliary spheroids on day 0, day 2, day 4, and day 6 after passage. **C,** Diameter (fold change) of the control and the *Smad4* silenced *HKβ* biliary spheroids ($n = 3$) on day 0, day 2, day 4, and day 6 after passage. Data are mean ± SEM. *, $P < 0.05$; **, $P < 0.01$, by Student *t* test. **D,** Microscopic images of DMSO, 1 μmol/L, and 10 μmol/L TGFβ inhibitor-treated *HKβ* biliary spheroids on day 0 and day 5 after treatment. **E,** Diameter (fold change) of DMSO, 1 μmol/L, and 10 μmol/L TGFβ inhibitor-treated *HKβ* biliary spheroids on day 1, day 3, and day 5 after treatment ($n = 3$/ group). Data are mean ± SEM. **F,** Relative gene expression of DMSO, 1 μmol/L, and 10 μmol/L TGFβ inhibitor-treated *HKβ* biliary spheroids on day 5 ($n = 3$/group). Data are shown as individual data points and the mean ± SEM. **E** and **F,** *, $P < 0.05$; **, $P < 0.01$; ***, $P < 0.001$, by one-way ANOVA with Dunnett's test (vs. DMSO). **G,** Xenograft tumors developed in five out of nine cases of *ShSmad4 HKβ* biliary spheroids, whereas no tumor developed in the controls ($n = 9$) 1 month after injection of spheroids. **H,** From the top, macroscopic images (one scale, 1 mm), H&E staining, immunostaining for CK19, Ki67, and Smad4, D-PAS staining of xenograft tumors derived from *Smad4*-silenced *HKβ* biliary spheroids. Scale bars, 50 μm (**A** and **H**) and 500 μm (**B** and **D**).

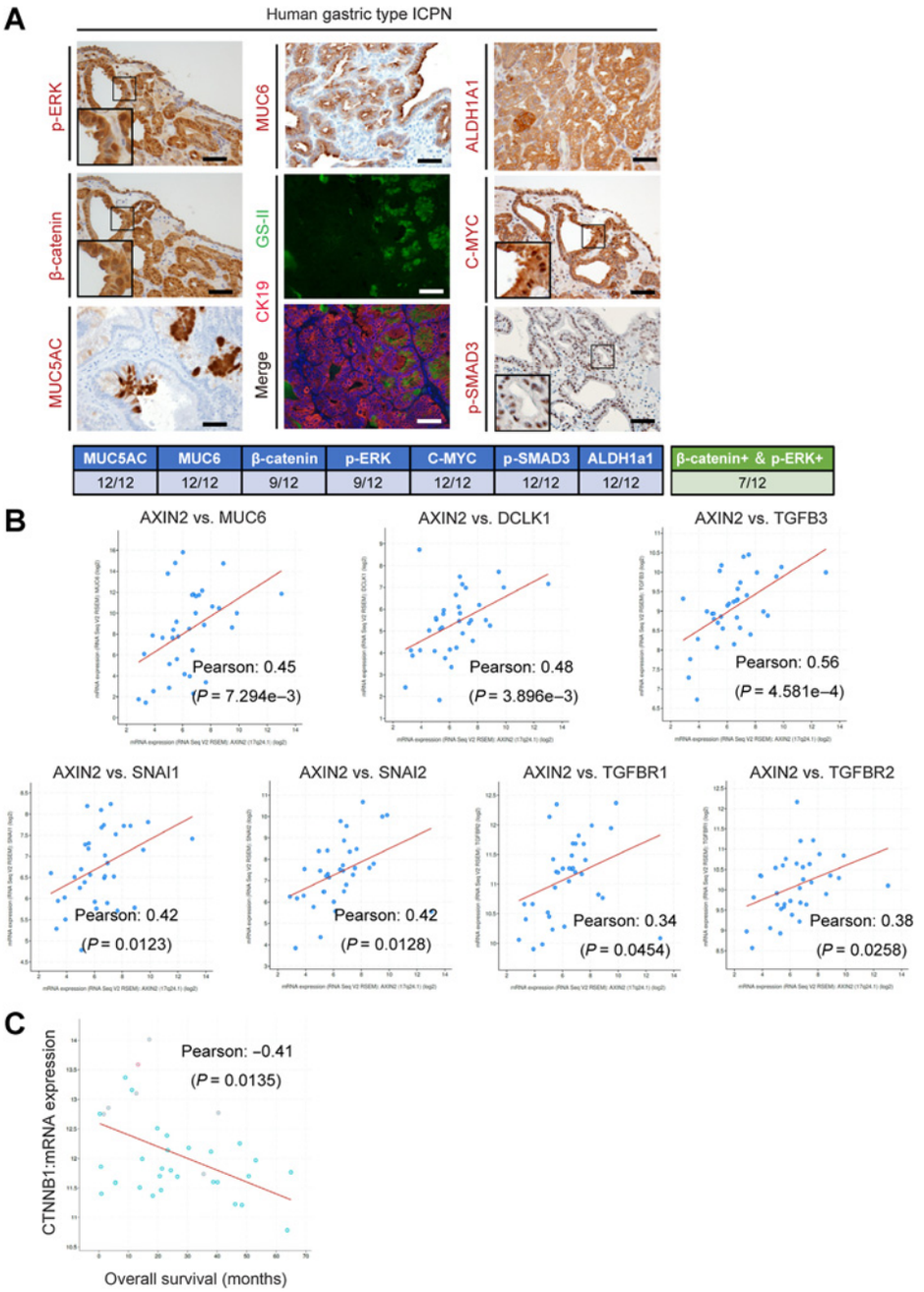

Figure 7.

Gene expression of human gastric type ICPN and human biliary cancer. **A,** From the top, immunostaining for p-ERK, β-catenin, MUC5AC, MUC6, GS-II (green), CK19 (red), DAPI (blue), ALDH1A1, C-MYC, and p-SMAD3 in human gastric type ICPN (n = 12). Scale bars, 50 μm. **B,** Genes positively correlated with AXIN2 expression in human biliary cancer by TCGA data analysis. **C,** Expression of CTNNB1 is negatively correlated with overall survival in human biliary cancer. **B** and **C,** Pearson correlation coefficient is described.

expressed GS-II (an alternate for MUC6), indicating the characteristics of the pyloric gland type, which was consistent with our mouse data. Moreover, in large agreement with our mouse data, ALDH1A1, C-MYC, and p-SMAD3 were also expressed in human ICPNs. These results further support our conclusion that murine BilIN and ICPN induced by biliary-specific concurrent activation of the Kras and Wnt pathways recapitulated human ICPNs.

To investigate whether ICPN of *HKβ* mice retained the characteristics of human biliary cancer in terms of gene expression, we performed correlative analyses using the TCGA database. Expression of *MUC6*, *DCLK1*, *SNAIL1*, *SNAIL2*, *TGFB3*, *TGFBR1*, and *TGFBR2* was positively correlated with *AXIN2* expression in human biliary cancer (**Fig. 7B**). Expression of *CTNNB1* was negatively correlated with overall survival in human biliary cancer (**Fig. 7C**). Therefore, these data further strengthen the human relevance of our mouse model, which provides direct evidence that concurrent activation of the Kras and Wnt pathways induces ICPN and BilIN, which could progress to biliary cancer.

Discussion

The WHO classification recently defined BilIN, IPNB, MCN, and ICPN as precancerous lesions of biliary cancer (7, 8, 10). However, it has not been demonstrated whether these lesions are bona fide

precursor lesions of biliary cancer. Moreover, the molecular mechanisms underlying the tumorigenesis of these precursor lesions and their driver mutations are not well understood. In this study, to determine the role of Kras and canonical Wnt pathways in tumorigenesis of the extrahepatic biliary tract including the EHBD and GB, we introduced endogenous expression of $KRAS^{G12D}$ and constitutive activation of Wnt signaling in the adult mouse biliary epithelium. We revealed that concurrent activation of the Kras and canonical Wnt pathways resulted in the development of biliary neoplasms that resembled human ICPNs and BilINs in the EHBD, putative precursors to biliary cancer. Furthermore, these lesions had the capacity to progress to adenocarcinomas in a xenograft model, establishing ICPNs and BilINs as precursors to biliary cancer. Thus, together with our analyses of the human clinical samples and the datasets described above, to the best of our knowledge, we have provided the first novel GEM that recapitulates human ICPN and BilIN, which can progress to biliary cancer.

In our global gene expression analysis of *HKβ* biliary spheroids, expression of c-Myc and the TGFβ pathway was upregulated in *HKβ* biliary spheroids. c-Myc is a known oncogene that promote progression of various types of cancer. Furthermore, it is one of the common downstream targets of Kras and Wnt pathways (33). In this study, we showed that silencing *c-Myc* or pharmacologic inhibition of c-Myc decreased the growth of *HKβ* biliary spheroids, suggesting the notion that c-Myc was a critical mediator for biliary tumorigenesis in *HKβ* mice. Moreover, consistent with our mouse data, we observed high c-MYC expression in human ICPN samples.

The TGFβ pathway works as a tumor suppressor in the early stage of tumorigenesis, whereas the TGFβ pathway induces EMT and function as a tumor suppressor in the late stage of tumorigenesis including pancreatic cancer (35, 36). In this study, we demonstrated that the silencing *Smad4*, silencing *Tgfbr2*, or pharmacologic inhibition of the TGFβ receptor increased the proliferation of *HKβ* biliary spheroids *in vitro*. Moreover, we showed that the silencing of *Smad4* or *Tgfbr2* markedly increased the progression of biliary cancer *in vivo*. Thus, concurrent activation of the Kras and Wnt pathways in the EHBD and GB resulted in an activated TGFβ pathway, which suppresses tumorigenesis and progression to biliary cancer. Consistent with our mouse data, we also revealed p-Smad3 expression, which is indicative of the activated TGFβ pathway, in human ICPN samples. Notably, SMAD4 expression was decreased in human high grade BilINs (37). Therefore, our data together with the previous report, suggest that the TGFβ pathway is an important barrier of ICPN and BilIN to progression to biliary cancer.

It is conceivable that co-activation of the Kras and canonical Wnt pathways upregulates TGFβ ligands, because pharmacological inhibition of the TGFβ receptor increased the proliferation of *HKβ* biliary spheroids *in vitro*. The TGFβ ligands include TGFβ1, 2, and 3. In our analysis of biliary spheroids, there were no differences in the expression of *TGFβ1* and *TGFβ2* among *H*, *HK*, *Hβ*, and *HKβ* biliary spheroids, whereas expression of *TGFβ3* was significantly higher in only *HKβ* biliary spheroids (**Fig. 3E**; Supplementary Fig. S9A). Therefore, it is most likely that concurrent activation of the Kras and Wnt pathways results in activation of the TGFβ pathway via the upregulation of the TGFβ3 ligand (Supplementary Fig. S10).

We showed that both UAE-1 and GS2 were expressed in ICPN and BilIN in *HKβ* mice. Although Muc1 was expressed in these neoplasms via IHC, *Muc1* expression in *HKβ* biliary spheroid was lower than that in control spheroids (Supplementary Fig. S9B and S9C). Our data suggested that concurrent activation of the Kras and canonical Wnt pathways in the EHBD and GB epithelium led to a decrease in the biliary characteristics, but increased the gastric characteristics including both the foveolar and pyloric gland types. Given that human IPNB also includes the gastric type, it would be interesting for future studies to investigate whether activation of the Wnt and Kras signaling pathways is also observed in gastric type human IPNB.

To our knowledge, we have demonstrated for the first time that $Hnf1b^{CreER}$ is a suitable biliary-specific CreER mouse line with high efficiency to perform genetic manipulation in the extrahepatic biliary system including the EHBD and GB. *Sox9CreER* (13) and *CK19CreER* mice (16) were previously used as a GEM in the analysis of the adult epithelium of the biliary tract. Sox9 is expressed in various organs, including chondrocytes, testis, heart, lung, pancreas, bile duct, hair follicles, retina, and the central nervous system (38). CK19 is expressed in the oral cavity, mammary gland, skin, gastrointestinal tract (from the esophagus to the rectum), and lung (39). Hnf1β is expressed in the gastrointestinal tract (from the stomach to the rectum), kidney, lung, and gonads (40). In this study, we found that *HKβ* mice died most likely due to massive intestinal adenomas. Therefore, massive intestinal adenomas would be also formed in *Sox9CreER;* $Kras^{G12D}$; $Ctnnb1^{lox(ex3)/+}$ and *CK19CreER;* $Kras^{G12D}$; $Ctnnb1^{lox(ex3)/+}$ mice, and thus, long-term analysis would be impossible similarly to *HKβ* mice. Therefore, we conclude that *Hnf1βCreER* line is one of the best lines for genetic manipulation in the extrahepatic biliary epithelium among several *CreER* mouse lines, including *Sox9CreER*, and *CK19CreER* lines.

Our lineage tracing analysis showed high efficiency of Cre expression in the epithelium of the EHBD and GB in $Hnf1b^{CreER}$*; Rosa26-LacZ* and $Hnf1b^{CreER}$*; Rosa26-tdTomato* mice. The difference in the efficiency of Cre recombination between $Hnf1b^{CreER}$*; Rosa26-LacZ* and $Hnf1b^{CreER}$*; Rosa26-tdTomato* is likely because the efficiency of reporter proteins is higher in *Rosa26-tdTomato* mice than in *Rosa26-LacZ* mice. It has been reported that the efficiency of Cre recombination of several reporter alleles varied greatly (41).

Finally, TCGA database analysis of human biliary cancer indicated a correlative relationship between the expression of AXIN2 and MUC6, DCLK1, EMT, and the TGFβ pathway. TCGA data indicated that biliary cancer in which the Wnt pathway is activated expresses MUC6. Thus, the Wnt signaling pathway could be a molecular therapeutic target for MUC6 positive biliary cancer. Future research should focus on revealing the functional role of the Kras and Wnt signaling pathways in established biliary cancer. and investigating whether Wnt signaling could be a therapeutic target for MUC6 positive biliary cancer

In summary, concurrent activation of the Kras and canonical Wnt pathways in the extrahepatic biliary system induced ICPN and BilIN, which can progress to biliary cancer. Mechanistically, c-Myc contributed to tumorigenesis, whereas the Tgfβ pathway inhibited it. Consistent with the mouse data, the Kras, Wnt signalings, c-Myc, and TGFβ pathway were activated in human ICPNs. We have provided the first novel GEM that recapitulates human ICPN and BilIN, establishing them precancerous lesions.

Authors' Disclosures

M. Nagao reports grants from grants-in-aid KAKENHI, Japan Agency for Medical Research and Development, the Project for Cancer Research and Therapeutic Evolution, AMED-PRIME, Moonshot Research and Development Program, COI-NEXT, Princess Takamatsu Cancer Research Fund, the Mochida Foundation, the Mitsubishi Foundation, the Uehara Foundation, the Naito Foundation, the Kobayashi Foundation, the Simizu Foundation, the Japan Foundation for Applied Enzymology,

the SGH Foundation, the Kanae Foundation, the Bristol Myers Squibb, the Ichiro Kanehara Foundation, and Takeda Foundation during the conduct of the study. M. Omatsu reports grants from JPMJSP2110 outside the submitted work. Y. Fukunaga reports other support from Sumitomo Dainippon Pharma Co., Ltd. during the conduct of the study. Y. Muta reports grants and personal fees from the Japan Society for the Promotion of Science during the conduct of the study. No disclosures were reported by the other authors.

Authors' Contributions

M. Nagao: Conceptualization, data curation, formal analysis, investigation, visualization, methodology, writing–original draft. **A. Fukuda:** Conceptualization, supervision, funding acquisition, methodology, project administration, writing–review and editing. **M. Omatsu:** Investigation. **M. Namikawa:** Investigation. **M. Sono:** Investigation. **Y. Fukunaga:** Investigation. **T. Masuda:** Investigation. **O. Araki:** Supervision. **T. Yoshikawa:** Investigation. **S. Ogawa:** Investigation. **K. Masuo:** Investigation. **N. Goto:** Investigation, methodology. **Y. Hiramatsu:** Funding acquisition, investigation. **Y. Muta:** Investigation, methodology. **M. Tsuda:** Investigation, methodology. **T. Maruno:** Investigation, methodology. **Y. Nakanishi:** Funding acquisition, investigation, methodology, writing–review and editing. **M. Taketo:** Resources. **J. Ferrer:** Resources. **T. Tsuruyama:** Investigation, he diagnosed murine neoplasia of biliary tract. **Y. Nakanuma:** Investigation, he diagnosed murine neoplasia of biliary tract. **K. Taura:** Resources. **S. Uemoto:** Resources. **H. Seno:** Supervision, funding acquisition, methodology, writing–review and editing.

Acknowledgments

This work was supported in part by grants-in-aid KAKENHI (19H03639, 19K16712, 19K22619, 20K22841, 20H03659, 21K15948, and 21K20801). It was also supported by Japan Agency for Medical Research and Development, the Project for Cancer Research and Therapeutic Evolution (18cm0106142h0001, 20cm0106177h0001, 20cm0106375h0001) and AMED-PRIME (20gm6010022h0003), Moonshot Research and Development Program (JPMJMS2022-1), and COI-NEXT (JPMJPF2018). It was also supported by Princess Takamatsu Cancer Research Fund (17-24924), the Mochida Foundation (2017bvAg), the Mitsubishi Foundation (201910037), the Uehara Foundation (201720143), the Naito Foundation (22205-1), the Kobayashi Foundation (203200700019), the Simizu Foundation (203180700103), the Japan Foundation for Applied Enzymology (203190700054), the SGH Foundation (203200700056), the Kanae Foundation (203190700083), the Bristol Myers Squibb (200190700011), the Ichiro Kanehara Foundation (20KI037), Takeda Science Foundation, and the Takeda Foundation (201749741, 203200700045). The authors thank all members of the Fukuda laboratory for technical assistance and helpful discussions.

The costs of publication of this article were defrayed in part by the payment of page charges. This article must therefore be hereby marked *advertisement* in accordance with 18 U.S.C. Section 1734 solely to indicate this fact.

Received July 7, 2021; revised December 31, 2021; accepted February 25, 2022; published first March 1, 2022.

References

1. Naghavi M. Europe PMC funders group the global burden of cancer 2013. JAMA Oncol 2015;1:505–27.
2. Rizvi S, Gores GJ. Pathogenesis, diagnosis, and management of cholangiocarcinoma. Gastroenterology 2013;145:1215–29.
3. Nagtegaal ID, Odze RD, Klimstra D, Paradis V, Rugge M, Schirmacher P, et al. The 2019 WHO classification of tumours of the digestive system. Histopathology 2020;76:182–8.
4. Lendvai G, Szekerczés T, Illyés I, Dóra R, Kontsek E, Gógl A, et al. Cholangiocarcinoma: classification, histopathology and molecular carcinogenesis. Pathol Oncol Res 2020;26:3–15.
5. Banales JM, Marin JJG, Lamarca A, Rodrigues PM, Khan SA, Roberts LR, et al. Cholangiocarcinoma 2020: the next horizon in mechanisms and management. Nat Rev Gastroenterol Hepatol 2020;17:557–88.
6. Hundal R, Shaffer EA. Gallbladder cancer: epidemiology and outcome. Clin Epidemiol 2014;6:99–109.
7. Zen Y, Adsay NV, Bardadin K, Colombari R, Ferrell L, Haga H, et al. Biliary intraepithelial neoplasia: an international interobserver agreement study and proposal for diagnostic criteria. Mod Pathol 2007;20:701–9.
8. Ohtsuka M, Shimizu H, Kato A, Yoshitomi H, Furukawa K, Tsuyuguchi T, et al. Intraductal papillary neoplasms of the bile duct. Int J Hepatol 2014;2014:1–10.
9. Nakanuma Y, Jang KT, Fukushima N, Furukawa T, Hong SM, Kim H, et al. A statement by the Japan-Korea expert pathologists for future clinicopathological and molecular analyses toward consensus building of intraductal papillary neoplasm of the bile duct through several opinions at the present stage. J Hepatobiliary Pancreat Sci 2018;25:181–7.
10. Adsay V, Jang KT, Roa JC, Dursun N, Ohike N, Bagci P, et al. Intracholecystic papillary-tubular neoplasms (ICPN) of the gallbladder (neoplastic polyps, adenomas, and papillary neoplasms that are ≥1.0 cm): clinicopathologic and immunohistochemical analysis of 123 cases. Am J Surg Pathol 2012;36:1279–301.
11. Nakamura H, Arai Y, Totoki Y, Shirota T, Elzawahry A, Kato M, et al. Genomic spectra of biliary tract cancer. Nat Genet 2015;47:1003–10.
12. Wardell CP, Fujita M, Yamada T, Simbolo M, Fassan M, Karlic R, et al. Genomic characterization of biliary tract cancers identifies driver genes and predisposing mutations. J Hepatol 2018;68:959–69.
13. Lin Y-K, Fang Z, Jiang T-Y, Wan Z-H, Pan Y-F, Ma Y-H, et al. Combination of Kras activation and PTEN deletion contributes to murine hepatopancreatic ductal malignancy. Cancer Lett 2018; 421:161–9.
14. Nakagawa H, Suzuki N, Hirata Y, Hikiba Y, Hayakawa Y, Kinoshita H, et al. Biliary epithelial injury-induced regenerative response by IL-33 promotes cholangiocarcinogenesis from peribiliary glands. Proc Natl Acad Sci U S A. 2017;114:E3806–15.
15. Kiguchi K, Carbajal S, Chan K, Beltrán L, Ruffino L, Shen J, et al. Constitutive expression of ErbB-2 in gallbladder epithelium results in development of adenocarcinoma. Cancer Res 2001;61:6971–6.
16. Hill MA, Alexander WB, Guo B, Kato Y, Patra K, O'Dell MR, et al. Kras and Tp53 mutations cause cholangiocyte- and hepatocyte-derived cholangiocarcinoma. Cancer Res 2018;78:4445–51.
17. Jusakul A, Cutcutache I, Yong CH, Lim JQ, Huang MN, Padmanabhan N, et al. Whole-genome and epigenomic landscapes of etiologically distinct subtypes of cholangiocarcinoma. Cancer Discov 2017;7:1116–35.
18. Hsu M, Sasaki M, Igarashi S, Sato Y, Nakanuma Y. KRAS and GNAS mutations and p53 overexpression in biliary intraepithelial neoplasia and intrahepatic cholangiocarcinomas. Cancer 2013;119:1669–74.
19. Pandey A, Stawiski EW, Durinck S, Gowda H, Goldstein LD, Barbhuiya MA, et al. Integrated genomic analysis reveals mutated ELF3 as a potential gallbladder cancer vaccine candidate. Nat Commun 2020;11:1–13.
20. Lin J, Peng X, Dong K, Long J, Guo X, Li H, et al. Genomic characterization of co-existing neoplasia and carcinoma lesions reveals distinct evolutionary paths of gallbladder cancer. Nat Commun 2021;12:1–11.
21. Goeppert B, Stichel D, Toth R, Fritzsche S, Loeffler MA, Schlitter AM, et al. Integrative analysis reveals early and distinct genetic and epigenetic changes in intraductal papillary and tubulopapillary cholangiocarcinogenesis. Gut 2021;71:391–401.
22. Solar M, Cardalda C, Houbracken I, Martín M, Maestro MA, De Medts N, et al. Pancreatic exocrine duct cells give rise to insulin-producing β cells during embryogenesis but not after birth. Dev Cell 2009;17:849–60.
23. Harada N, Tamai Y, Ishikawa TO, Sauer B, Takaku K, Oshima M, et al. Intestinal polyposis in mice with a dominant stable mutation of the β-catenin gene. EMBO J 1999;18:5931–42.
24. Nakanishi Y, Seno H, Fukuoka A, Ueo T, Yamaga Y, Maruno T, et al. Dclk1 distinguishes between tumor and normal stem cells in the intestine. Nat Genet 2013;45:98–103.
25. Miyoshi H, Stappenbeck TS. In vitro expansion and genetic modification of gastrointestinal stem cells as organoids. 2008;42:157–62.
26. Rodrigo-Torres D, Affò S, Coll M, Morales-Ibanez O, Millán C, Blaya D, et al. The biliary epithelium gives rise to liver progenitor cells. Hepatology 2014;60:1367–77.
27. Shimizu T, Choi E, Petersen CP, Noto JM, Romero-Gallo J, Piazuelo MB, et al. Characterization of progressive metaplasia in the gastric corpus mucosa of Mongolian gerbils infected with Helicobacter pylori. J Pathol 2016;239:399–410.
28. Buzzelli JN, Chalinor HV, Pavlic DI, Sutton P, Menheniott TR, Giraud AS, et al. IL33 is a stomach alarmin that initiates a skewed Th2 response to injury and infection. Cell Mol Gastroenterol Hepatol 2015;1:203–21.

29. Goto N, Ueo T, Fukuda A, Kawada K, Sakai Y, Miyoshi H, et al. Distinct roles of HES1 in normal stem cells and tumor stem-like cells of the intestine. Cancer Res 2017;77:3442–54.
30. Yoshino J, Akiyama Y, Shimada S, Ogura T, Ogawa K, Ono H, et al. Loss of ARID1A induces a stemness gene ALDH1A1 expression with histone acetylation in the malignant subtype of cholangiocarcinoma. Carcinogenesis 2020;41:734–42.
31. Massagué J. How cells read TGF-β signals. Nat Rev Mol Cell Biol 2000;1: 169–78.
32. Coffinier C, Barra J, Babinet C, Yaniv M. Expression of the vHNF1/HNF1β homeoprotein gene during mouse organogenesis. Mech Dev 1999;89:211–3.
33. Dang CV. MYC on the path to cancer. Cell 2012;149:22–35.
34. Zirath H, Frenzel A, Oliynyk G, Segerström L, Westermark UK, Larsson K, et al. MYC inhibition induces metabolic changes leading to accumulation of lipid droplets in tumor cells. Proc Natl Acad Sci U S A 2013; 110:10258–63.
35. Roberts AB, Wakefield LM. The two faces of transforming growth factor β in carcinogenesis. Proc Natl Acad Sci U S A 2003;100:8621–3.
36. Lüttges J, Galehdari H, Bröcker V, Schwarte-Waldhoff I, Henne-Bruns D, Klöppel G, et al. Allelic loss is often the first hit in the biallelic inactivation of the p53 and DPC4 genes during pancreatic carcinogenesis. Am J Pathol 2001; 158:1677–83.
37. Nakanishi Y, Zen Y, Kondo S, Itoh T, Itatsu K, Nakanuma Y. Expression of cell cycle–related molecules in biliary premalignant lesions: biliary intraepithelial neoplasia and biliary intraductal papillary neoplasm. Hum Pathol 2008;39:1153–61.
38. Furuyama K, Kawaguchi Y, Akiyama H, Horiguchi M, Kodama S, Kuhara T, et al. Continuous cell supply from a Sox9-expressing progenitor zone in adult liver, exocrine pancreas and intestine. Nat Genet 2011;43:34–41.
39. Chu PG, Weiss LM. Keratin expression in human tissues and neoplasms: other issues. Histopathology 2003;43:196–7.
40. Yu DD, Guo SW, Jing YY, Dong YL, Wei LX. A review on hepatocyte nuclear factor-1beta and tumor. Cell Biosci 2015;5:1–8.
41. Liu J, Willet SG, Bankaitis ED, Xu Y, Wright CVE, Gu G. Non-parallel recombination limits cre-loxP-based reporters as precise indicators of conditional genetic manipulation. Genesis 2013;51:436–42.